Coordinated Hydrolysis Explains the Mechanical Behavior of Kinesin

Charles S. Peskin* and George Oster‡

*Courant Institute of Mathematical Sciences, New York, New York 10012, and ‡Department of Molecular and Cellular Biology, University of California, Berkeley, California 94720 USA

ABSTRACT The two-headed motor protein kinesin hydrolyzes nucleotide to move unidirectionally along its microtubule track at speeds up to 1000 nm/s (Saxton et al., 1988) and develops forces in excess of 5 pN (Hunt et al., 1994; Svoboda et al., 1994a). Individual kinesin molecules have been studied recently in vitro, and their behavior has been characterized in terms of force-velocity curves and variance measurements (Svoboda and Block, 1994a; Svoboda et al., 1994b). We present a model for force generation in kinesin in which the ATP hydrolysis reactions are coordinated with the relative positions of the two heads. The model explains the experimental data and permits us to study the relative roles of Brownian motion and elastic deformation in the motor mechanism of kinesin.

INTRODUCTION

Any mechanism that proposes to explain the operation of the motor protein kinesin is constrained by the following recent observations: (i) the protein moves unidirectionally along a microtubule protofilament (Ray et al., 1993); (ii) it can achieve speeds of nearly 1000 nm/s at low loads, decreasing to zero velocity at a stall force between 5 and 6 pN, which is practically independent of ATP concentration (Hunt et al., 1994; Svoboda and Block, 1994a); (iii) the variance in its trajectories at low loads increases linearly with time at a rate significantly below that expected for a Poisson stepping process (Svoboda et al., 1994b). Indeed, Svoboda et al. have measured the entire force-velocity curve at several ATP concentrations (Svoboda and Block, 1994a). These data, along with their experiments measuring the growth of the trajectory variance, provide a strong constraint on proposed mechanisms.

Biochemical studies generally measure only the aggregate hydrolysis rate of all of the ATPase sites. Recently, however, efforts have been made to distinguish between the ATPase rates of each head, and they do not appear to be operating independently (Gilbert et al., 1995; Hackney, 1994; Johnson et al., 1994). Here we present a model in which coordinated hydrolysis naturally occurs.[1]

One question common to all motor models is the relative roles of Brownian motion and elastic deformation energy in transducing chemical bond energy into a directed force. Some models of molecular motors rest almost entirely on rectifying Brownian diffusion to produce a thrust, or torque (Cordova et al., 1991; Huxley, 1957; Meister et al., 1989; Peskin et al., 1993). Such models cease to operate at zero temperature. Others ascribe the displacement of the motor to a "power stroke" in the form of a conformational change in the motor induced by nucleotide binding and/or hydrolysis (Finer et al., 1994; Rayment et al., 1994) or by binding to the microtubule track (Huxley and Simmons, 1971). Models of this sort continue to operate at zero temperature. (Of course, hydrolysis would cease as $T \to 0$, hence these statements apply only to the models.) This is a fundamental issue in understanding motor function, but it is extremely difficult to resolve experimentally (Hunt et al., 1994). The model we present incorporates both conformational and Brownian contributions, so that we can investigate the dominant contribution of each mechanism. We find that, to fit the experimental data, there must be an elastic (e.g., enthalpic) deformation that moves each head at least 80% of the distance between binding sites, the remaining distance being accomplished by Brownian diffusion.

DESCRIPTION OF THE MODEL

Fig. 1 shows the essentials of the mechanical model. We assume that only one head of the motor can bind to each β-tubulin site at a time. These sites are located at a distance $L = 8$ nm apart. The two heads of the motor are connected at a hinge. We assume that the hinge swings freely within its range of motion but that this range is limited so that the distance between the heads as measured along the microtubule cannot be greater than L. The two heads can freely pass each other. As in the experiments of Svoboda et al., the motor tows a latex bead, which is joined to the hinge of the motor by an elastic tether. A load force, f, opposing the motion of the motor, is applied to the bead by a laser trap (Svoboda and Block, 1994a).

In the model, each head of the motor has two possible tubulin affinity states, denoted **S** and **W**. In state **S**, the head has a high affinity for the β-tubulin sites. It will bind to the first empty site that it encounters and remain there until a transition to state **W** occurs. In state **W**, the head has a low affinity for the β-tubulin sites; it diffuses along the microtubule and is oblivious to these sites, not binding even if it encounters an empty one.

[1] There is no direct evidence that a single-headed kinesin or dynein molecule, acting alone, can drive a load. However, Gelles et al. (1994) have reported that several single-headed kinesins can move a microtubule in an in vitro assay. These single heads are mechanically coupled via the microtubule, so the motion of one influences the others.

Address reprint requests to Dr. George Oster, University of California, 201 Wellman Hall, Berkeley, CA 94720-3112. Tel.: 510-642-5277; Fax: 510-642-5277; E-mail: goster@nature.berkley.edu.

0006-3495/95/04/202s/10 $2.00

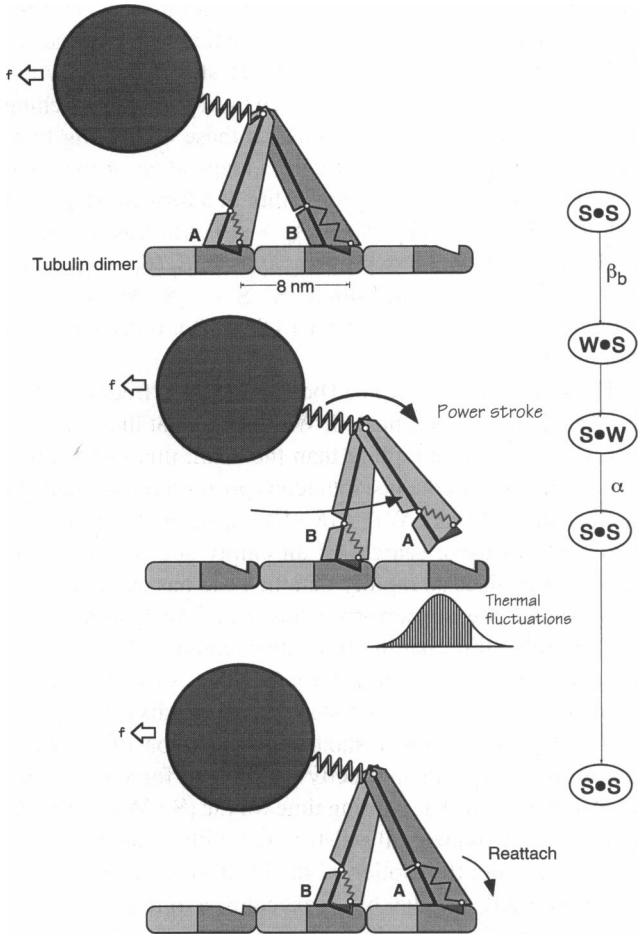

FIGURE 1 The mechanical model consists of two heads joined by a free hinge attached to a bead by an elastic linkage. The heads face in the same direction, which defines the forward direction of the motor as a whole. We assume that the microtubule track has discrete sites, located 8 nm apart, at which the kinesin heads may bind reversibly (the asymmetry of the binding sites is indicated by their shape). Only one head at a time may be bound to any given site, and we assume that the size of the heads and the hinge connecting them makes it impossible for the heads to reach more than 8 nm apart. Thus, the only way that both heads can be bound is if they occupy adjacent sites on the tubulin polymer. Finally, we assume that the two heads can move freely past each other, like the legs of a person walking. The elasticity of the heads is modeled by a pair of linear "ankle" springs, whose strain state is indicated by their shading (light = unstrained, dark = strained). The model setup is intended to mimic the experimental setup of Svoboda and Block (1994); however, the drawings are not to scale. The top panel shows the motor in state $\mathbf{S} \cdot \mathbf{S}$. The back head is in its forward-leaning state (the gray spring is relaxed); the front head, because it is hinged to its partner, is forced into its backward-leaning state (the strain is indicated by a black spring). In the elastic potential well of the bead-motor linkage, the bead is subject to Brownian fluctuations. (*middle*) The motor can make forward progress by detaching the back head (entering state $\mathbf{W} \cdot \mathbf{S}$), whereupon the front head relieves its strain by swinging forward; this is the power stroke (and puts the motor in state $\mathbf{S} \cdot \mathbf{W}$). At some point, the head regains its affinity for the track, and the motor reenters state $\mathbf{S} \cdot \mathbf{S}$. The new forward head then rapidly diffuses to the first empty site it encounters (in the lower panel this is shown as the forward site). Note that this sequence represents an 8-nm step for the motor as a whole, because the average position of the two heads has advanced 8 nm. Note that the act of docking has put head A into a strained configuration. Alternatively, the motor can make an 8-nm backward step (not shown) by picking up the front head, swinging it backwards, and reattaching it to the track.

The transition from state $\mathbf{S} \rightarrow \mathbf{W}$ involves ATP hydrolysis. We shall assume that the hydrolysis rate is greater for the back head than for the front head. This is one of the two mechanisms that drives the motor forward. The other mechanism involves the geometry of a kinesin head bound to the microtubular track (in state **S**). We assume that the preferred configuration of the bound head is one in which the head leans forward. When the motor has *both* heads bound, the back head is in this favorable configuration, but the front head is forced into a strained, backward-leaning configuration because of its hinged connection to the back head. This strain on the front head is relieved when the back head switches to its weak-binding state and detaches. Then the front head, still in state **S**, can relax by rotating forward and pulling the formerly back head forwards. This is the "power stroke" of the motor's mechanical cycle.[2]

THE MECHANOCHEMICAL CYCLE

We can now describe the mechanical cycle of the motor as follows (Fig. 1). We start from the state $\mathbf{S} \cdot \mathbf{S}$, in which both heads are bound to the microtubule at adjacent sites, 8 nm apart. In this state, the motor is rigid and the latex bead undergoes Brownian motion in the potential well established by the elastic tether of the bead to the hinge of the motor. The next event that can happen is the transition $\mathbf{S} \rightarrow \mathbf{W}$, in which one of the two heads detaches. As explained above, this requires ATP hydrolysis, and the transition is more likely to occur in the back head. This could occur, for example, because the strain induced in the front head adversely affects its hydrolysis site, slowing or arresting its catalytic activity. Once a head is in state **W**, it is free to move, and a coupled Brownian motion of that head and the bead occurs. The potential energy of this coupled Brownian motion involves not only the elastic tether that connects the bead to the hinge, but also the elasticity of the bound head (i.e., the spring in Fig. 1) that favors the forward-leaning configuration of the head in state **S**. The motion of the free head is restricted to the interval $(-L, L)$ with respect to the position of the bound head. This situation persists until the transition $\mathbf{W} \rightarrow \mathbf{S}$ occurs, at which point the free head recovers its high affinity for the (empty) binding sites on the microtubule.[3] The free head then binds to the first site that it encounters. The two sites that are within reach are the ones 8 nm in front and 8

[2] Note that the hand-over-hand gait we have assumed requires that the forward head generates the power stroke by pulling the rear head. This is unlike macroscopic walking, which is "ballistic" (i.e., depends on inertia). Without inertia, the rear head cannot contribute to the power stroke once it detaches.

[3] Another possibility in this situation is that the one remaining bound head hydrolyzes ATP and makes the transition $\mathbf{S} \rightarrow \mathbf{W}$. Then the motor is in the state $\mathbf{W} \cdot \mathbf{W}$ and dissociates from the microtubule. Such events are in fact observed (Svoboda and Block, 1994a). Their probability can be kept low in the model by assuming that the rate of the $\mathbf{S} \rightarrow \mathbf{W}$ transition depends on the angle of the bound head in such a way that the rate is low at the intermediate angles likely to be assumed by a bound head when the other head is freely diffusing along the microtubule. For purposes of this paper, we assume that the transition $\mathbf{S} \cdot \mathbf{W} \rightarrow \mathbf{W} \cdot \mathbf{W}$ does not occur.

nm in back of the bound head. It is biased toward the more posterior of these sites by the applied load, but toward the more anterior site by the forward-leaning tendency of the bound head.

Although the mechanical cycle does not uniquely determine the kinetics, Fig. 2 shows how the mechanical cycle in Fig. 1 is consistent with the kinetic scheme proposed by Gilbert et al. (Gilbert et al., 1995; Johnson and Gilbert, 1994). The key parameters of the model are:

- β_b = unbinding rate constant for the back head $\mathbf{S} \rightarrow \mathbf{W}$
- β_f = unbinding rate constant for the front head $\mathbf{S} \rightarrow \mathbf{W}$
- α = rebinding rate constant for either head $\mathbf{W} \rightarrow \mathbf{S}$
- L = distance between the binding sites on the microtubule
- x_0 = equilibrium position of the hinge with respect to the bound head when only one head is bound. We define the power stroke as the distance the free head moves from its original position to get to that equilibrium position (power stroke = $L + 2x_0$).
- f = applied load

The two asymmetries that drive the motor are (i) $\beta_b > \beta_f$, which expresses the greater ATPase activity of the back head of the motor, and (ii) $x_0 > 0$, which expresses the forward-leaning tendency of a bound kinesin head; this generates the "power stroke" of the motor. The first of these inequalities makes the back head more likely to detach, and the second one makes it more likely to reattach as a front head. Under the combined influence of these two asymmetries, the motor marches systematically forward.

ANALYSIS AND SIMULATION OF THE MODEL

We have numerically simulated the motion of a single two-headed kinesin molecule towing a latex bead against an applied load. The direction in which the motor steps, and the waiting times between steps, are stochastically determined as follows. In state $(\mathbf{S} \cdot \mathbf{S})$ the motor can step forward by detaching its back head, and it can step backward by detaching its front head. The rate constants for these competing transitions are β_b and β_f, respectively, independent of the position of the bead. Thus, the probability of a forward step from state $(\mathbf{S} \cdot \mathbf{S}) \rightarrow (\mathbf{S} \cdot \mathbf{W})$, is $\beta_b/(\beta_b + \beta_f)$, whereas the probability of a backward step of this type is $\beta_f/(\beta_b + \beta_f)$. The waiting time for the transition $(\mathbf{S} \cdot \mathbf{S}) \rightarrow (\mathbf{S} \cdot \mathbf{W})$ is exponentially distributed with mean $1/(\beta_b + \beta_f)$, independent of the direction of the step.

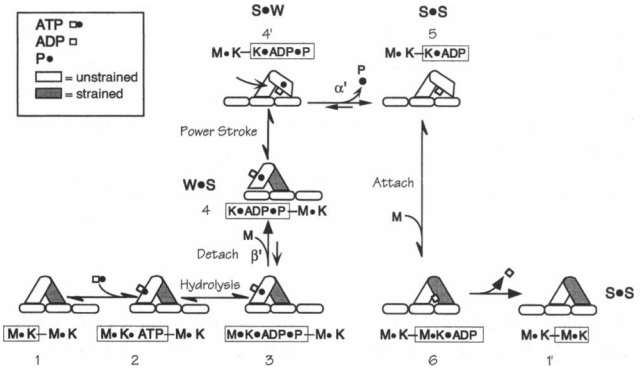

FIGURE 2 The mechanical cycle mapped onto the kinetic cycle proposed by Gilbert and Johnson (1994a, b). Their pathway for a single head is shown boxed. When the two heads are joined by a hinge, their cycles are correlated. The diagram shows one possible sequence of states wherein the energy for driving the power stroke derives from the binding free energy of the motor to the tubulin track, analogous to the Huxley-Simmons model for myosin (Huxley and Simmons, 1971). Fast reactions are indicated by double arrows, whereas slow reactions are indicated by separate arrows. The model parameters α and β can be determined from the kinetic parameters α' and β' by taking into account the equilibrium constants of the fast reactions.

The situation with one head bound, the other free (i.e., state $(\mathbf{S} \cdot \mathbf{W})$) is more complicated. We assume that the free head diffuses much more rapidly than the bead; this implies that it equilibrates with the instantaneous position of the bead. At the instant of the $(\mathbf{S} \cdot \mathbf{W}) \rightarrow (\mathbf{S} \cdot \mathbf{S})$ transition, the free head begins its diffusive search for an empty site. Because this search takes place so rapidly that the bead has essentially no time to move, we can perform a "fast scale" analysis to evaluate the probability that the first site encountered is the front site and, hence, that the transition $(\mathbf{S} \cdot \mathbf{W}) \rightarrow (\mathbf{S} \cdot \mathbf{S})$ is a forward rather than a backward step (see Appendix). This probability depends on the instantaneous position of the bead (therefore, it depends indirectly on the load force that is applied to the bead). The waiting time for the $(\mathbf{S} \cdot \mathbf{W}) \rightarrow (\mathbf{S} \cdot \mathbf{S})$ transition is exponentially distributed with mean $1/\alpha$.

Now consider the motion of the bead. In state $(\mathbf{S} \cdot \mathbf{S})$, the motor is rigid, so the bead executes a one-dimensional Brownian motion in a given potential. In state $(\mathbf{S} \cdot \mathbf{W})$, the Brownian motions of the bead and the free head are coupled. Because the diffusion coefficient of the free head is much greater than that of the bead, we can compute a free energy that serves as the effective potential for the Brownian motion of the bead in state $(\mathbf{S} \cdot \mathbf{W})$. Thus, in both states the bead executes Brownian motion in a potential. The particular potential felt by the bead, however, varies depending on the state and position of the kinesin motor to which it is attached.

The foregoing ideas can be used not only to simulate the motion of an individual kinesin motor but also to analyze the behavior of an ensemble of such motors. To do the analysis, however, we make one further simplifying assumption: that the diffusion time of the bead over distances on the order of 8 nm is brief in comparison with the mean lifetimes of the states $\mathbf{S}$ and $\mathbf{W}$, i.e., the reaction rates α and β that summarize the hydrolysis cycle are slow in comparison with the rate of diffusion of the bead over the step length of the motor. Under this assumption, we no longer need to track the diffusion of the bead, but can instead average over bead positions appropriately weighted by the equilibrium position density of the bead. In particular, we average over the positions of the bead when computing the probability that a free head will find a front or a back binding site when it reattaches to the track. This reduces the motion of kinesin to a Markov chain, for which we can calculate the mean displacement and also the rate of growth of the variance in the position of the motor, as time goes by.

In the Appendix, we compute the following simple expression for the mean velocity of the motor

$$\langle v(f)\rangle = \underbrace{\frac{\delta}{2}\left(\frac{\alpha L}{\alpha+\gamma}\right)}_{\text{Reaction asymmetry}} + \underbrace{\gamma\left(\frac{\alpha L}{\alpha+\gamma}\right)\left(P(f)-\frac{1}{2}\right)}_{\text{Power stroke}} \tag{1}$$

where $\gamma = \beta_b + \beta_f$ is the total hydrolysis rate of both heads and $\delta = \beta_b - \beta_f$ is the difference in the rate of hydrolysis between the two heads. The quantity $P(f)$ is the probability that a head that has just made the $\mathbf{W} \rightarrow \mathbf{S}$ transition (i.e., has regained its high affinity) will find the empty binding site in front of the bound head instead of the one behind the bound head. Because the load, f, opposes the motion, P is a decreasing function of f.[4] For a particular experiment at constant load, P is a constant.

In addition to the mean velocity, higher moments can be calculated; in the Appendix, we derive an expression for the growth rate of the variance:

$$\frac{d}{dt}\mathrm{var}(f) = \frac{L^2}{2}\frac{\alpha\gamma}{\alpha+\gamma} \cdot \left[1 - \frac{4\left(\alpha\left(P(f)-\frac{1}{2}\right)-\frac{\delta}{2}\right)\left(\gamma\left(P(f)-\frac{1}{2}\right)-\left(\frac{\alpha\delta}{2\gamma}\right)\right)}{(\alpha+\gamma)^2}\right]. \tag{2}$$

RESULTS

Fig. 3 shows a simulated trajectory of a bead attached to the motor. This sample path reflects the stochastic motion of the bead-motor assembly. The motor is stepping in 8-nm increments; however, if the bead-motor spring is too weak, it is difficult to discern those steps because they are concealed in the Brownian fluctuations of the bead. Using the laser trap, Svoboda and Block were able to stiffen effectively the bead spring and reveal the underlying stepping dynamics. The trajectory in Fig. 3 was generated with a stiffer bead spring than the force-velocity and variance calculations (see below) to reveal the steps.

Fig. 4 shows the fits of the model to the force-velocity data of Svoboda and Block (2) at high (2 mM) and low (10 μM) ATP concentrations. The model was initially fit to the high [ATP] data using experimentally determined values for all parameters except for the reaction rate asymmetry parameter, δ, and the mechanical asymmetry parameter, x_0. Then to fit the data for the low [ATP] force-velocity curve, only the net reaction rate, γ, was changed while holding the ratio β_f/β_b constant (so that δ changes in proportion to γ). To fit the force-velocity data, we found that it was necessary to impose both a reaction rate ratio $\beta_f/\beta_b \leq 0.05$, and also a power stroke that would carry the free head at least 80% of the distance to the next binding site; neither asymmetry by itself would suffice to fit the data.

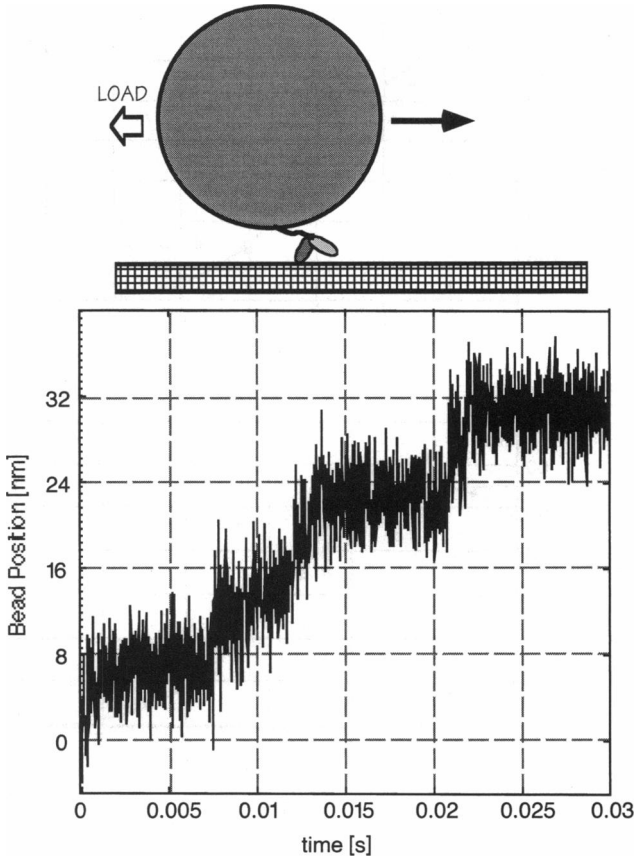

FIGURE 3 A stochastic simulation of the model equations illustrating the statistical nature of the motor's progress. In this simulation, the time step was 7×10^{-7} s; the plot shows computed points sampled every 0.1 ms. The 8-nm steps are not discernible if the bead-motor spring is weak so that the steps are concealed in the bead's thermal fluctuations; therefore, in this simulation the bead-motor linkage was assigned the stiffness $K_b = 0.8$ pN/nm, which is greater than the values used in Figs. 4 and 5, so that the stepping dynamics would be clearly visible.

Fig. 5 shows the fit of the model to the variance data of Svoboda et al. (1994b). If the kinesin motor were progressing by random Poisson steps of length L at rate β_b, then the variance in its position would grow linearly with time at a rate $L^2\beta_b$ (see the discussion after Eq. A.30 in the Appendix). The actual rate, both for kinesin and for the model, is considerably less than this, an indication that more than one rate-limiting step is involved in each 8-nm step of the motor. At present, only low load variance data are available. If variance data were collected at several loads, those data, together with the force-velocity data that are already available, would provide a severe constraint on the model parameters and, indeed, a severe test of the model itself.

DISCUSSION

Fitting the model to the above data imposes two constraints on the operation of the motor. First, elastic deformation of the bound kinesin head (the "power stroke") accomplishes at

[4] P also depends on the size of the power stroke and the elastic stiffness of the heads and of the bead-motor linkage.

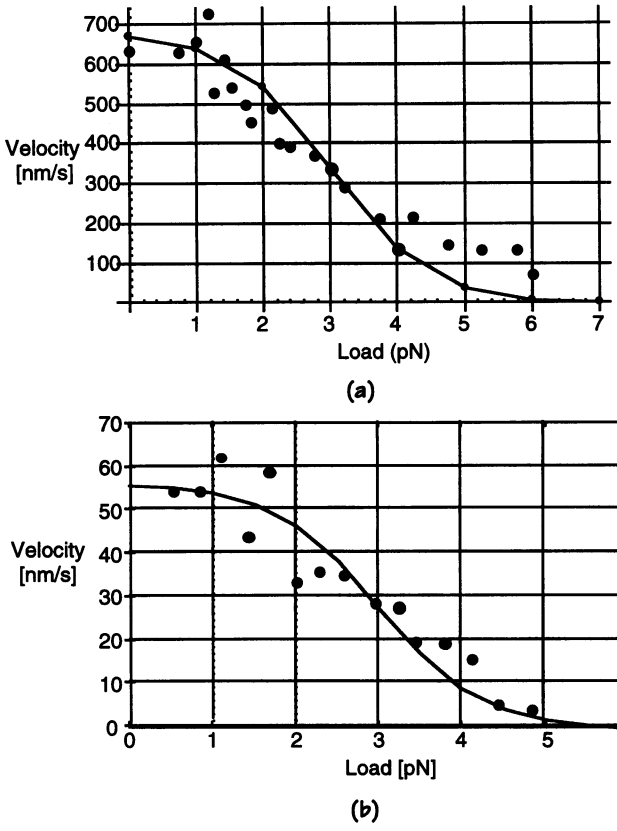

FIGURE 4 The predicted load velocity curves from Eq. 1 for high (2 mM) (*top*) and low (10 μM) ATP concentrations (*bottom*). The data are from Svoboda and Block (1994). The parameter values used to fit the data were: $\alpha = 400\ s^{-1}$, $\gamma = 105\ s^{-1}$, $\delta = 100\ s^{-1}$, K_b (stiffness of bead-motor linkage) = 0.25 pN/nm (Svoboda and Block, 1994), $x_0 = 3$ nm (corresponding to a power stroke of 14 nm), K_m (head elasticity) = 1 pN/nm. All parameters are the same for the two data sets except that the net hydrolysis rate, γ, was decreased from 105 to 11 s^{-1}, while maintaining the ratio β_f/β_b constant. Note the S-shaped character of the force-velocity curve: the kinesin motor is insensitive to load at low loads, and this aspect of its dynamics is captured by the model.

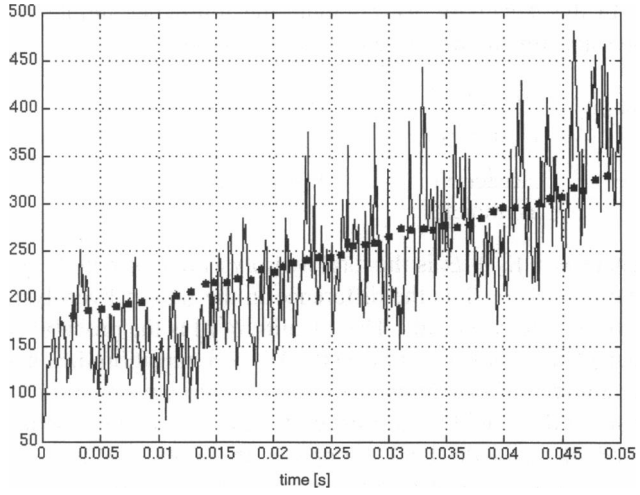

FIGURE 5 Comparison of simulated trajectory variance (*erratic line*) to the measured trajectory variance (●) (4). The least-squares slope of the experimental data is 3120 nm^2/s, and the slope of the variance predicted by Eq. 2 is 3560 nm^2/s. A Poisson stepper would have a slope of $\beta_b L^2 = 6400$ nm^2/s. All parameters are the same as in *b* except that here $K_b = 0.03$ pN/nm. The real bead-motor linkage acts like a nonlinear spring, so its stiffness is load-dependent. The variance measurements in (4) were made at low load.

least 80% of the step, the remaining 20% being supplied by thermal motion. Thus, it is clear that a substantial elastic shape change is required to bias the motor's walk sufficiently to generate the observed force-velocity behavior. The uncertainty as to the exact values for the head elasticity and the bead-motor connection do not affect this very much, because altering their values over a wide range could not compensate for too small a power stroke. Second, fitting the model to the data requires that the rear head be at least 20 times more likely to bind and/or hydrolyze its ATP than is the front head; the model is insensitive to asymmetries much above this level.

The principle enunciated here is simple: a pair of elastically coupled ATPases can function as a powerful motor if their individual asymmetries and the manner in which they are coupled makes a forward step more likely than a backward one. We have suggested two mechanisms for this: hydrolysis reaction asymmetry and an elastically driven power stroke. Although either is sufficient to drive the motor forward, both are needed to fit the data. Both mechanisms are related to the angle that a bound kinesin head makes with the track. When both heads are bound, the geometry of the motor as a whole dictates that the back head is leaning forward whereas the front head is leaning backward. We assume that a head leaning forward is more likely to hydrolyze ATP and hence to detach, and that the forward-leaning configuration has a lower free energy than the backward-leaning configuration. This leads to a preferred sequence of events in which the back (forward-leaning) head binds and splits ATP, and detaches from the track. Once this has happened, the front (backward-leaning) head is free to relax by rotating forward, and this biases the diffusion of the free head in the forward direction. This makes the free head more likely to find the binding site 8 nm in front of the bound head, not the site 8 nm behind the bound head, where it started.

Why should a forward-leaning kinesin head hydrolyze ATP faster than a backward-leaning head? It is known that kinesin bound to tubulin is a far more effective ATPase than kinesin alone, and it is likely that the ATP-binding site is close to the tubulin-binding site, as it is in myosin (Rayment et al., 1993). Therefore, it is likely that the ATPase site interacts strongly with the tubulin-binding site on a kinesin head. Thus, it would not be surprising if the ATPase activity depended on the specific geometry of the kinesin-microtubule interaction.

The success of the asymmetric reaction rate model gives encouragement to the view that other molecular motors may operate on the same principle.The pivoting cross-bridge picture is almost irresistible for kinesin, myosin, and dynein, given their molecular geometries (Rayment and Holden, 1994; Rayment et al., 1993); however, for other motors the geometry is not so suggestive. For example, DNA and RNA

polymerases present no obvious protuberances; however, they are multimeric and hydrolyze nucleotide at a high rate. Therefore, it is worth considering the possibility that these motors operate by two or more hydrolysis sites whose activities are correlated. Indeed, Vale has noted that for many progressive enzymes it appears necessary to coordinate the binding activities of several sites on different subunits (Vale, 1994). This hypothesis finds precedent in the multiple, coordinated hydrolysis sites found to control the opening and closing of the CFTR chloride channel (Anderson et al., 1992; Hwang et al., 1993; Nagel et al., 1994). Finally, we note that both Hackney (1994) and Gilbert and Johnson (1994, 1995) have found evidence from kinetic studies that the two kinesin heads alternate their hydrolysis cycles. Our mechanical study complements and reinforces their conclusions.

We thank K. Svoboda, S. Block, and S. Gilbert for sharing their data with us, and S. Block for valuable conversations and suggestions.
Both authors were supported by National Science Foundation grant NSF FD92–20719.

APPENDIX

Derivation of the model equations

Consider the model shown in Fig. 1. Two heads are connected by a hinge to which is attached a large bead by a spring. The motor is asymmetrical, so that we can distinguish the front from the back. The track is also asymmetrical; the motor and the track fit together such that the motor faces in the direction of increasing x.

The track has equally spaced binding sites separated by a distance L = 8 nm. Only one head may bind to a given site, and the heads may move freely past one another. The coordinates of the heads are $x = x_1$ and $x = x_2$. The hinge is always located halfway between the heads: $x_h = (x_1 - x_2)/2$. We assume that the hinge swings freely within its range of motion, but that it imposes the constraint: $|x_1 - x_2| \le L$.

The motor tows a 0.5-μm bead whose coordinate is denoted x_3. The bead is connected to the hinge by a linear spring of stiffness K_b. A load force, f, is applied to the bead (positive to the left). Let D_3 be the diffusion coefficient of the bead. We condense the hydrolysis cycle into two states, which we denote 0 and 1, with transition rate constants shown in Fig. 6 *a*.

In state 0, a head can glide freely along the track and does not interact with the binding sites. In state 1, the head binds to the first empty site it encounters. Once bound, it remains bound at the same site until the transition $1 \rightarrow 0$ occurs.

We shall assume that the rate constant for the transition $1 \rightarrow 0$ depends on the angle that the bound head makes with the track; this angle is determined by the relative position of the hinge and the head. Note that

$$\beta_1 = \beta(x_h - x_1) = \beta(\tfrac{1}{2}(x_1 + x_2) - x_1) = \beta[(x_2 - x_1)/2] \qquad \text{(A1)}$$

and

$$\beta_2 = \beta(x_h - x_2) = \beta(\tfrac{1}{2}(x_1 + x_2) - x_2) = \beta[(x_1 - x_2)/2] \qquad \text{(A2)}$$

This provides a mechanism of interaction between the two heads. For example, suppose that β is an increasing function; then $x_1 < x_2$ implies $\beta_1 > \beta_2$. This means that the back head is more likely to detach than the front head.

If we ignore the labels "1" and "2" of the heads, the motor as a whole has but three distinguishable states: 11, 01≡10, and 00. In state 00, however, both heads are free, and the motor dissociates from the track, terminating the walk. Therefore, we need consider only states 11 and 01≡10. The possible transitions and the progress of the motor can be depicted as shown in Fig. 6 *b*.

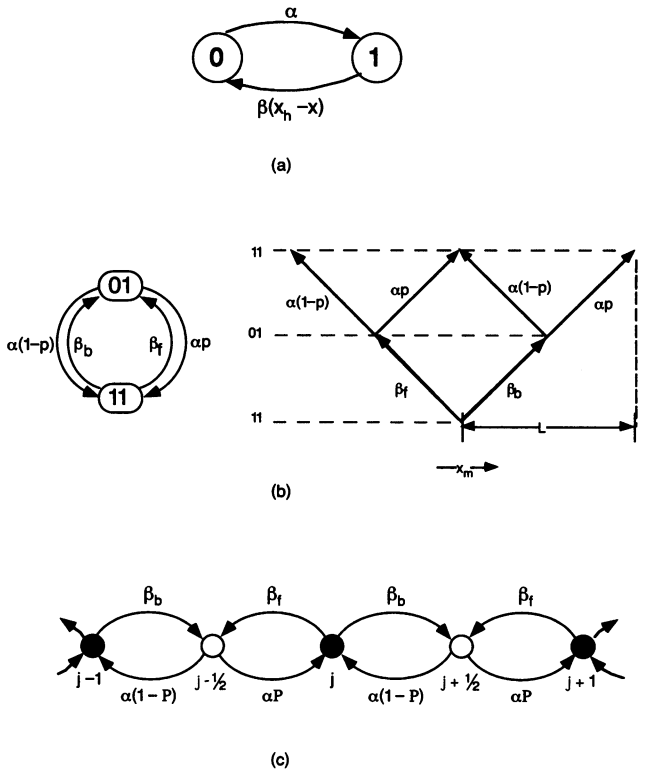

FIGURE 6 Schematic of the model geometry (not to scale). (*a*) The state transition diagram for a single head. 0 is the detached state, and 1 the attached state. α is the attachment rate constant, and β is the detachment rate constant, which may depend on the angle of the head as measured by the longitudinal displacement of the hinge from the head, $x_h - x$. (*b*) (*left*) The transition diagram between the two states (01) and (11). β_f and β_b are the rate constants for detaching the front and back head from the track, respectively. In state 01, when only one head is bound, there is another possibility (not shown) in which the single-bound head detaches, terminating the walk. We shall ignore this possibility here, although it is easily included. α is the rate constant for binding the free head to the track, and p is the probability that it binds in *front* of the bound head (so that $1 - p$ is the probability of binding in back of the front head). Clockwise arrows denote forward progress of the motor, and counterclockwise arrows represent backwards progress. (*right*) The probability branching diagram showing the progress of the motor. We define the motor position, x_m, as the position of the *hinge* when both heads are bound (state 11) and the position of the *bound* head when only one head is bound (state 01). Thus, x_m changes in increments of $\pm L/2$ during the transitions. Over a full cycle, $11 \rightarrow 11$, however, the change in x_m is 0 or $\pm L$. (*c*) The Markov chain describing the movement of the motor. State j denotes $x_m = jL$. Integer values of j (*filled circles*) correspond to states with both heads bound; half-integer values correspond to states with one head bound.

To determine the motion of the bead, we must give a more detailed analysis of states 11 and 01 and derive expressions for the rate constants of the transitions, some of which depend on the position of the bead.

State 11: both heads bound

In this state, the motor is rigid; its heads occupy adjacent sites on the track and the hinge is halfway between them. Let x_m be the position of the hinge. Then the front head is at $x_m + L/2$ and the back head is at $x_m - L/2$. In this configuration, the bead diffuses with diffusion coefficient D_3 in the potential of the bead-motor spring:

$$\phi_{11}(x_3, x_m) = f(x_3 - x_m) + \tfrac{1}{2}K_b(x_3 - x_m)^2 \qquad \text{(A3)}$$

The rate constants for leaving state 11 are as follows:

detachment rate of back head:

$$\beta_b = \beta(x_m - (x_m - L/2)) = \beta(L/2) \tag{A4}$$

detachment rate of front head:

$$\beta_f = \beta(x_m - (x_m + L/2)) = \beta(-L/2) \tag{A5}$$

State 01≡10: one head bound, one head free

In state 11, x_m was the coordinate of the hinge. However, in state 01 we redefine x_m as:

$$x_m = \text{coordinate of the bound head.}$$

and we set

$$x = \text{coordinate of the free head.}$$

Thus, x_m jumps $\pm L/2$ during any transition between state 01 and state 11. Between transitions, x_m is constant.

Although the motor is in state 01, we have a coupled diffusion involving the free head (located at x) and the bead (located at x_3), on the domain given by $x_m - L \le x \le x_m + L$ and $-\infty < x_3 < \infty$. The potential energy of this coupled diffusion process is

$$\phi_{01}(x, x_3, x_m) = f(x_3 - x_m) + \frac{K_b}{2}\left(\frac{x + x_m}{2} - x_3\right)^2 + W\left(\frac{x + x_m}{2} - x_m\right) \tag{A6}$$

$$= f(x_3 - x_m) + \frac{K_b}{2}\left(\frac{x - x_m}{2} - (x_3 - x_m)\right)^2 + W\left(\frac{x - x_m}{2}\right).$$

Here W is the potential energy of the interaction between the bound head and the track. This depends on the angle of the head, which is determined by the relative position of the hinge with respect to the bound head. The second form of ϕ_{01} in the above equation emphasizes the fact that $\phi_{01}(x, x_3, x_m)$ actually depends only on the two variables $x - x_m$ and $x_3 - x_m$.

We can simplify the model considerably by considering the situation in which the diffusion coefficient, D, of the free head is much larger than the diffusion coefficient of the bead, D_3. In fact, we shall let $D \to \infty$. In this limit, the free head equilibrates instantaneously, forming a probability cloud over the interval $[x_m - L, x_m + L]$ according to the Boltzmann density function:

$$\rho(x \mid x_3, x_m) = \frac{\exp\left(-\dfrac{\phi_{01}(x, x_3, x_m)}{k_B T}\right)}{\displaystyle\int_{-X_m - L}^{X_m + L} \exp\left(-\frac{\phi_{01}(x', x_3, x_m)}{k_B T}\right) dx'} \tag{A7}$$

where k_B is Boltzmann's constant and T is the absolute temperature. The notation $\rho(x \mid x_3, x_0)$ indicates that this is a *conditional* probability density function, given x_3 and x_m. As x_3 changes because of the bead diffusion, the probability cloud shifts.

In this limit, it can be shown that the bead diffuses with diffusion coefficient D_3 as though it were in the effective potential (free energy) given by

$$\Phi_{01}(x_3, x_m) = -k_B T \log \int_{x_m - L}^{x_m + L} \exp\left(-\frac{\phi_{01}(x, x_3, x_m)}{k_B T}\right) dx. \tag{A8}$$

This determines the statistical motion of the bead throughout the duration of state 01.

The rate constant for the rebinding of the free head to the track is given by the constant α. But we must determine whether the head binds at $x_m + L$ or at $x_m - L$. Let

$p(x_3, x_m)$ = probability that the free head binds at $x = x_m + L$

$1 - p(x_3, x_m)$ = probability that the free head binds at $x = x_m - L$

where x_3 is the position of the bead and x_m is the position of the bound head at the instant when the transition to the high affinity state occurs. We can compute $p(x_3, x_m)$ from the following considerations.

As soon as the free head enters the high affinity state, it diffuses rapidly until it encounters an empty site on the track, whereupon it binds. The two sites available to it are at the ends of its diffusion interval, $x_m \pm L$. On the time scale of the average motor motion, this process is essentially instantaneous ($D \to \infty$); however, we can analyze it on a *fast* time scale as follows.[5]

Let τ denote the fast-scale time measured from the instant that the free head enters the strong binding state, and let $c(x, \tau \mid x_3, x_m)$ and $J(x, \tau \mid x_3, x_m)$ be the probability density and probability flux, respectively, of the free head for $\tau > 0$. On the fast scale of τ, the positions of the bead, x_3, and the bound head, x_m, are constant. c and J obey the following conservation equation:

$$\frac{\partial c}{\partial \tau} = -\frac{\partial J}{\partial x}, \qquad J = -D\left(\frac{\partial c}{\partial x} + \frac{1}{k_B T} c \frac{\partial \phi_{01}}{\partial x}\right),$$

$$c(x, 0 \mid x_3, x_m) = \rho(x \mid x_3, x_m), \tag{A9}$$

$$c(x_m - L, \tau \mid x_3, x_m) = c(x_m + L, \tau \mid x_3, x_m) = 0.$$

The probability of binding to the next site, rather than the previous site, is computed from

$$p(x_3, x_m) = \int_0^\infty J(x_m + L, \tau \mid x_3, x_m)\, d\tau. \tag{A10}$$

To obtain this, we integrate the diffusion equation with respect to τ over $(0, \infty)$ and introduce the quantity

$$F(x \mid x_3, x_m) = \int_0^\infty J(x, \tau \mid x_3, x_m)\, d\tau. \tag{A11}$$

The absorbing boundary condition implies $c \to 0$ as $\tau \to \infty$, and so

$$0 - \rho(x \mid x_3, x_m) + \frac{\partial F}{\partial x}(x \mid x_3, x_m) = 0. \tag{A12}$$

From this it follows that

$$F(x \mid x_3, x_m) = F(x_m + L \mid x_3, x_m) - \int_x^{x_m + L} \rho(x' \mid x_3, x_m)\, dx' \tag{A13}$$

$$= p(x_3, x_m) - \int_x^{x_m + L} \rho(x' \mid x_3, x_m)\, dx'$$

From the definition of the flux, J, we have

$$J \exp\left(\frac{\phi_{01}}{k_B T}\right) = -D\frac{\partial}{\partial x}\left(c \exp\left(\frac{\phi_{01}}{k_B T}\right)\right)$$

$$\int_{x_m - L}^{x_m + L} J \exp\left(\frac{\phi_{01}}{k_B T}\right) dx = 0 \tag{A14}$$

$$\int_{x_m - L}^{x_m + L} F(x \mid x_3, x_m) \exp\left(\frac{\phi_{01}}{k_B T}\right) dx = 0$$

The last step was obtained by integrating with respect to time from 0 to infinity. This may also be written

$$\int_{x_m - L}^{x_m + L} F(x \mid x_3, x_m)\, \sigma(x \mid x_3, x_m)\, dx = 0 \tag{A15}$$

[5] The binding of the head to the tubulin site is electrostatic and hydrophobic, so binding cannot take place until the head diffuses within about a Debye length of the site (<1 nm).

where

$$\sigma(x \mid x_3, x_m) = \frac{\exp\left(\dfrac{\phi_{01}(x, x_3, x_m)}{k_B T}\right)}{\displaystyle\int_{x_m - L}^{x_m + L} \exp\left(\frac{\phi_{01}(x', x_3, x_m)}{k_B T}\right) dx'}. \quad \text{(A16)}$$

Substituting (A.13) into (A.15) we obtain

$$p(x_3, x_m) = \int_{x_m - L}^{x_m + L} \sigma(x \mid x_3, x_m) \int_{x}^{x_m + L} \rho(x' \mid x_3, x_m)\, dx'\, dx. \quad \text{(A17)}$$

It can be checked that $p(x_3, x_m)$ actually depends only on the single variable $x_3 - x_m$. This formula expresses the influence of the bead on whether the free head binds in front of, or behind, the bound head.

The model equations in the limit of fast bead diffusion

For a 0.5-μm bead diffusing against a 0.5 pN/nm spring, the time to diffuse the 8-nm distance between binding sites is very small: $\tau_D \approx 10^{-5}$ s. Thus, the bead diffusion can be taken as much faster than the hydrolysis cycle:

$$\alpha \ll 2D_3/L^2; \qquad \beta(y) \ll 2D_3/L^2, \qquad -L/2 \le y \le L/2 \quad \text{(A18)}$$

then we may assume that the bead equilibrates rapidly with the effective potential that it feels in each state. Accordingly, we can average over all possible positions of the bead, which simplifies the model considerably. This averaging has no influence on state 11 (both heads bound), because in this state the bead itself has no influence on the motion of the motor. In state 01 or 10 (one head bound, one free), however, the position of the bead does influence the probability that the free head will reattach in front of the bound head. This relationship was determined above (Eq. A.17).

Recall that $p(x_3, x_m)$ actually depends only on the displacement $x_3 - x_m$, which we shall henceforth denote X. We express this by writing $p(x_3, x_m) = \hat{p}(x_3 - x_m) = \hat{p}(X)$. Likewise, $\Phi_{01}(x_3, x_m) = \hat{\Phi}_{01}(x_3 - x_m) = \hat{\Phi}_{01}(X)$. Now the equilibrium probability density function for the bead in the effective potential $\hat{\Phi}_{01}$ is given by

$$\hat{p}_{01}(X) = \frac{\exp(-\hat{\Phi}_{01}(X)/k_B T)}{\int_{-\infty}^{\infty} \exp(-\hat{\Phi}_{01}(X)/k_B T)\, dX'}. \quad \text{(A19)}$$

This probability density can be used to compute the overall probability that the free head binds in front of the back head:

$$P(f) = \int_{-\infty}^{\infty} \hat{p}_{01}(X)\hat{p}(X)\, dX. \quad \text{(A20)}$$

Note that P depends of several parameters including the load force, f.

Now $x_m(t)$ is a sample path of a Markov process with the state diagram shown in Fig. 6 *c*. Let $C_j(t)$ be the probability of finding the system in state j at time t. For integer values of j, $C_j(t)$ and $C_{j+1/2}(t)$ obey the following equations

$$\frac{dC_j}{dt} = \alpha P C_{j-1/2} + \alpha(1 - P)C_{j+1/2} - (\beta_b + \beta_f)C_j \quad \text{(A21)}$$

$$\frac{dC_{j+1/2}}{dt} = \beta_b C_j + \beta_f C_{j+1} - \alpha C_{j+1/2}. \quad \text{(A22)}$$

From these, we can derive equations for the moments

$$M_k = \sum_{j=-\infty}^{\infty} j^k C_j \qquad N_k = \sum_{j=-\infty}^{\infty} \left(j + \frac{1}{2}\right)^k C_{j+1/2}. \quad \text{(A23)}$$

The moment equations are:

$$\frac{d}{dt}\begin{pmatrix} M_0 \\ N_0 \end{pmatrix} = \begin{pmatrix} -(\beta_b + \beta_f) & \alpha \\ (\beta_b + \beta_f) & -\alpha \end{pmatrix}\begin{pmatrix} M_0 \\ N_0 \end{pmatrix} \quad \text{(A24)}$$

$$\frac{d}{dt}\begin{pmatrix} M_1 \\ N_1 \end{pmatrix} = \begin{pmatrix} -(\beta_b + \beta_f) & \alpha \\ (\beta_b + \beta_f) & -\alpha \end{pmatrix}\begin{pmatrix} M_1 \\ N_1 \end{pmatrix} + \begin{pmatrix} 0 & \alpha(P - \tfrac{1}{2}) \\ (\beta_b - \beta_f)/2 & 0 \end{pmatrix}\begin{pmatrix} M_0 \\ N_0 \end{pmatrix} \quad \text{(A25)}$$

$$\frac{d}{dt}\begin{pmatrix} M_2 \\ N_2 \end{pmatrix} = \begin{pmatrix} -(\beta_b + \beta_f) & \alpha \\ (\beta_b + \beta_f) & -\alpha \end{pmatrix}\begin{pmatrix} M_2 \\ N_2 \end{pmatrix} + \begin{pmatrix} 0 & 2\alpha(P - \tfrac{1}{2}) \\ (\beta_b - \beta_f) & 0 \end{pmatrix}\begin{pmatrix} M_1 \\ N_1 \end{pmatrix} + \begin{pmatrix} 0 & \alpha/4 \\ (\beta_b + \beta_f)/4 & 0 \end{pmatrix}\begin{pmatrix} M_0 \\ N_0 \end{pmatrix} \quad \text{(A26)}$$

The steady-state solutions for (M_0, N_0) that normalize to $M_0 + N_0 = 1$ are:

$$M_0 = \frac{\alpha}{\alpha + \beta_b + \beta_f}, \qquad N_0 = \frac{\beta_b + \beta_f}{\alpha + \beta_b + \beta_f} \quad \text{(A27)}$$

Adding the equations for M_1 and N_1, we find the mean velocity of the motor, $L(d/dt)(M_1 + N_1)$, which simplifies to:

$$\boxed{\langle v \rangle = \frac{\alpha L}{2(\alpha + \gamma)}\left[\delta + 2\left(P - \frac{1}{2}\right)\gamma\right]} \quad \text{(A28)}$$

where $\gamma \equiv \beta_b + \beta_f$, $\delta \equiv \beta_b - \beta_f$, and where P is computed from the integral (A.20). In the limit $P \to 1$, $\beta_f \to 0$, $\alpha \to \infty$, the motion of the motor becomes a Poisson birth process with mean velocity $\langle v \rangle = L\beta_b$.

Evaluation of the variance is more difficult. We have

$$\text{var} = L^2[(M_2 + N_2) - (M_1 + N_1)^2]$$

$$\frac{d}{dt}\text{var} = L^2\left[\frac{d}{dt}(M_2 + N_2) - 2(M_1 + N_1)\frac{d}{dt}(M_1 + N_1)\right]$$

After some algebra, we find:

$$\frac{d}{dt}\text{var} = \frac{1}{2}\frac{\alpha\gamma}{\alpha + \gamma} + 2M_0N_0\left[\frac{\delta}{2} - \alpha\left(P - \frac{1}{2}\right)\right]\left[\frac{M_1}{M_0} - \frac{N_1}{N_0}\right].$$

Now the steady values of M_0 and N_0 have already been given above: $M_0 = \alpha/(\alpha + \gamma)$, $N_0 = \gamma/(\alpha + \gamma)$, and a separate computation using the first-moment equations shows that

$$\lim_{t\to\infty}\left(\frac{M_1}{M_0} - \frac{N_1}{N_0}\right) = \frac{(P - \tfrac{1}{2})\gamma - (\alpha/\gamma)(\delta/2)}{\alpha + \gamma}.$$

Combining these results, we find that

$$\boxed{\lim_{t\to\infty}\frac{d}{dt}\text{var} = \frac{L^2}{2}\frac{\alpha\gamma}{\alpha + \gamma}\left[1 - \frac{4(\alpha(P - \tfrac{1}{2}) - \delta/2)(\gamma(P - \tfrac{1}{2}) - (\alpha/\gamma)(\delta/2))}{(\alpha + \gamma)^2}\right]} \quad \text{(A29)}$$

Thus, after an initial transient, the variance of the kinesin trajectories should settle down to a straight line, var ~ constant + slope × t, with the slope given by the right-hand side of Eq. A.29.

Although it is not obvious by inspection, one can show (as a check) that the right-hand side of Eq. A.29 is nonnegative, so the variance cannot decrease over time.

It is instructive to consider the special case $P = 1$ and $\beta_f = 0$, in which the motor marches inexorably forward. Then

$$\langle v \rangle = L \frac{\alpha\beta_b}{\alpha + \beta_b}$$
$$\frac{d}{dt}\text{var} = \frac{1}{2} L\langle v \rangle \left(1 + \left(\frac{\alpha - \beta_b}{\alpha + \beta_b}\right)^2\right) \quad \text{(A30)}$$

which is minimized by setting $\alpha = \beta_b$, and maximized by letting $\alpha \to \infty$ or $\beta_b \to \infty$. The minimum and maximum values are $\frac{1}{2}L\langle v \rangle$ and $L\langle v \rangle$, respectively, $\frac{1}{2}L\langle v \rangle \leq (d/dt)\text{var} \leq L\langle v \rangle$. Note that $L\langle v \rangle$ characterizes a Poisson stepping process. This shows in a simple case how the two-step hydrolysis cycle can reduce the variance of the kinesin trajectories. If the rate of increase of the variance were measured as a function of load and/or ATP concentration, such experiments would provide further data to constrain and test the model.

REFERENCES

Anderson, M., and M. Welsh. 1992. Regulation by ATP and ADP of CFTR chloride channels that contain mutant nucleotide-binding domains. *Science.* 257:1701–1704.

Cordova, N., B. Ermentrout, and G. Oster. 1991. The mechanics of motor molecules. I. The thermal ratchet model. *Proc. Natl. Acad. Sci. USA.* 89:339–343.

Finer, J., R. Simmons, and J. Spudich. 1994. Single myosin molecule mechanics: piconewton forces and nanometre steps. *Nature.* 368:113–119.

Gelles, J. et al. 1994. Structural and functional features of one- and two-headed biotinated kinesin derivatives. *In* Molecular Motors: Structure, Mechanics and Energy Transduction. Biophysical Society, Airlie, VA.

Gilbert, S., M. Webb, M. Brune, and K. Johnson. 1995. Kinesin crossbridge detachment occurs after ATP hydrolysis. *Nature.* In press.

Hackney, D. 1994. Evidence for alternating head catalysis by kinesin during microtubule-stimulated ATP hydrolysis. *Proc. Natl. Acad. Sci. USA.* 91: 6865–6869.

Hunt, A., F. Gittes, and J. Howard. 1994. The force exerted by single kinesin molecule against a viscous load. *Biophys. J.* 67:766–781.

Huxley, A. F. 1957. Muscle structure and theories of contraction. *Prog. Biophys. biophys. Chem.* 7:255–318.

Hwang, T. C., M. Horie, and D. Gadsby. 1993. Functionally distinct phosphoforms underlie incremental activation of protein kinase-regulated Cl^- conductance in mammalian heart. *J. Gen. Physiol.* 101:629–650.

Johnson, K., and S. Gilbert. 1994. Pathway of the microtubule-kinesin ATPase. *In* Molecular Motors: Structure, Mechanics and Energy Transduction. Biophysical Society, Airlie, VA.

Meister, M., S. R. Caplan, and H. C. Berg. 1989. Dynamics of a tightly coupled mechanism for flagellar rotation: bacterial motility, chemiosmotic coupling, protonmotive force. *Biophys. J.* 55:905–914.

Nagel, G., T. C. Hwang, A. Nairn, and D. Gadsby. 1994. AMP-PNP Delays the closing of CFTR Cl^- channels opened by ATP. *Biophys. J.* 66:141*a*. (Abstr.)

Peskin, C., G. Odell, and G. Oster. 1993. Cellular motions and thermal fluctuations: the Brownian ratchet. *Biophys. J.* 65:316–324.

Ray, S., E. Meyhofer, R. Milligan, and J. Howard. 1993. Kinesin follows the microtubule's protofilament axis. *J. Cell Biol.* 121:1083–1093.

Rayment, I., and H. Holden. 1994. The three-dimensional structure of a molecular motor. *TIBS.* 129–134.

Rayment, I. et al. 1993. Three-dimensional structure of myosin subfragment-1: a molecular motor. *Science.* 261:50–58.

Saxton, W. et al. 1988. Drosophila kinesin: characterization of microtubule motility and ATPase. *Proc. Natl. Acad. Sci. USA.* 85:1109–1113.

Svoboda, K., and S. Block. 1994a. Force and velocity measured for single kinesin molecules. *Cell.* 77:773–784.

Svoboda, K., P. Mitra, and S. Block. 1994b. Fluctuation analysis of motor protein movement and single enzyme kinetics. *Proc. Natl. Acad. Sci. USA.* In press.

Vale, R. 1994. Getting a grip on myosin. *Cell.* 78:733–737.

DISCUSSION

Session Chairperson: Steven Block
Scribe: F. Jon Kull

MALCOLM IRVING: At the end of your chapter in the study book, you say this could be adapted to myosin. I wonder if you could say briefly what kind of changes you would have to make in this scheme.

GEORGE OSTER: A lot . . . it turns out. At least with this kind of stochastic model, the proportion of brownian motion is a lot higher in myosin, because myosin spends most of its time off. It sort of slaps the actin whereas kinesin kind of grabs it and then lets go and then quickly rebinds. And so it turns out with that kind of cycle, the model changes quite a bit and we have not done all of the simulations so I don't want to say too much about it. But it is different. That is to say, in our hands the myosin looks much more Brownian driven than elastically driven.

STAN LEIBLER: I have two short questions. How many parameters do you have in your model, exactly? And, the second question is, what are the data you cannot explain with your model? Do you expect any data which you will not be able to explain?

OSTER: The model parameters are the difference in reaction rate between the front and back head, the step size (we used an 8-nm step but you can try various stepping patterns), and the total hydrolysis rate, which is a complicated partition function. The dependence on load and power stroke is a complicated partition function as well.

LEIBLER: But this is a function?

OSTER: Well, it is a number once you carry out the integration.

LEIBLER: In this equation it is a function . . .

OSTER: Yes, in this equation it is a function. But when you put in a power stroke and the load, then you get a number. By the way, the formula for the mean velocity nicely partitions into contributions from the reaction asymmetry and the contribution by the power stroke. What was the other question? What can't I explain? Well, there is probably a lot I can't explain. [Steven Block suggests that the model will not explain God.]

LEIBLER: Other than that, you can explain everything?